The assessment of field ionization detectors for molecular beam use

2004 J. Phys.: Condens. Matter 16 S2863

(http://iopscience.iop.org/0953-8984/16/29/002)

INSTITUTE OF PHYSICS PUBLISHING JOURNAL OF PHYSICS: CONDENSED MATTER

J. Phys.: Condens. Matter **16** (2004) S2863–S2878 PII: S0953-8984(04)80477-6

The assessment of field ionization detectors for molecular beam use

R B Doak

Department of Physics and Astronomy, Arizona State University, Tempe, AZ 85287-1504, USA

Received 4 May 2004
Published 9 July 2004
Online at stacks.iop.org/JPhysCM/16/S2863
doi:10.1088/0953-8984/16/29/002

Abstract

An overly simplistic but nonetheless useful model is employed to explore basic attributes of field ionization detection. The base cross-sectional detection area of a field ionization tip is set by a centrifugal barrier: molecules impinging at too high a velocity or too large an impact parameter cannot reach the tip and therefore cannot be ionized. For those that do reach the tip, the probability of ionization depends critically on whether they lose sufficient energy on their initial impact to be captured in the polarization field of the tip. Capture is enhanced if the tip radius lies well within the centrifugal barrier and the impinging species is highly polarizable. Scaling relations are developed within the context of this model, allowing recent measurements of field ionization yields to be assessed.

1. Motivation

The field of molecular beams has yet to develop a detector that is universal *and* efficient *and* fast. The notable achievements in molecular beam research over the last several decades are a tribute to the high spectral intensity of modern supersonic free-jet expansions rather than to any exceptional detection capabilities. Conventional fast universal molecular beam detectors, based on electron impact (EI) ionization, typically detect only one particle in 10^4–10^6 [1]. Attempts to improve EI detection efficiency invariably introduce other detector limitations. The highest EI efficiency to date, 7×10^{-3} [2], was obtained by confining the ionizing electrons magnetically to an extended ionization region. This degrades temporal response, however, and would severely limit the time-of-flight (TOF) velocity analysis employed in many molecular beam experiments. Multi-photon ionization, which is now possible with commercial lasers, does offer 100% ionization probability even for helium [3], and is extremely fast since the pulse length of such lasers is very short (∼100 fs). The pulse repetition rate, however, is very slow (∼1 kHz) so that the overall time-averaged detection efficiency is only about 10^{-10}. If a small, fast, and efficient universal beam detector could be developed, it would be a boon not just to the molecular beam community but to mass spectrometry in general.

Field ionization (FI) has long been an attractive basis for such a detector. Seminal molecular beam detection by field ionization was carried out in the 1960s and 1970s [4–6]. The results were encouraging but further development of a field ionization detector (FID) was never pursued. The principle is simple [7]. A high positive electric potential is placed on a needle having a tip radius of 10–50 nm. This produces a strong electric field near the tip, rising to a maximum of a few tens of volts per nanometre at the tip surface. Atoms or molecules entering this inhomogeneous E-field are polarized and drawn towards the tip, where an electron can tunnel into the needle. The resulting positive ion accelerates outwards to be mass selected and detected. The crucial and necessary occurrences are (1) that an impinging molecule reach the tip and (2) that an electron tunnel into the tip. Relevant to the first event is a 'centrifugal barrier' imposed by conservation of angular momentum. Molecules impinging with too much energy or at too large an impact parameter will not reach the tip and hence cannot be ionized. A related question is whether a molecule might reach the tip by means other than direct impingement from the gas. Relevant to the second event is the probability of capture of the molecule in the polarization field of the tip. The probability of electron tunnelling into the tip peaks in a narrow region a few ångströms outside the tip surface. If a molecule becomes trapped in the polarization field, it will pass repeatedly through this tunnelling region and must eventually be ionized, if not on the first impact then on subsequent bounces. This paper explores these issues in the context of a very simple model.

Field ionization is a 'soft' ionization technique, meaning that ionization transpires with little or no fragmentation of the analyte molecule[1]. It is therefore uniquely suited to mass spectrometry of large and complex organic molecules, including biologically relevant molecules. Conventional electron impact (EI) ionization, in contrast, invariably causes significant dissociative ionization. Even if the EI cracking pattern of the analyte species is known, deconvolution and interpretation of EI mass spectra is correspondingly more complicated. A single FI tip delivers very little signal intensity due to its intrinsically small ionization volume. Accordingly, a large array of tips is needed to provide usable signal levels for mass spectrometry. Clusters of carbon whiskers can be grown for this purpose by a variety of means [8] or even purchased commercially[2]. Carbon nanotubes are of possible interest as FI whiskers [9]. Modern microfabrication techniques—such as photolithography and/or electron beam lithography in conjunction with thin film deposition and anisotropic reactive ion etching—allow fabrication of ordered microscopic arrays of FI tips [10]. The overall efficiency of such FI arrays reportedly approaches that of electron impact ionization sources [10]. Stability and reproducibility of ionization is a major concern with all FI tips, and this problem is compounded in tip arrays or clusters. Techniques are being developed to clean and anneal tip arrays [11], but the problem will probably not be fully solved until arrays of individually addressable tips become available. FI arrays offer, in principle, two-dimensional (2D) detection capability for molecular beams. A 2D detector for neutral beams does not currently exist. Its attainment would be a tremendous technological advance for all beam–beam and beam–surface scattering experiments.

Given this perspective, field ionization detection of molecular beams clearly merited another look. The immediate motivations were two-fold:

(1) The state of the art of molecular beam sources had advanced tremendously since the 1960s and 1970s, with high speed ratio supersonic beams supplanting the effusive sources of that

[1] The technological relevance of this is hard to overstate. ESI and MALDI, two of the methods for delivering unfragmented protein ions into a mass spectrometer were heralded with the 2002 Nobel Prize in Chemistry. A discussion of ionization techniques may be found at http://www.jeol.com/ms/docs/ionize.html

[2] For example, Linden-CMS, Auf dem Berge 25, D-28844 Leeste, Germany; http://www.fdms.de/

earlier era. The very narrow velocity distribution of a supersonic beam greatly extends the scope of experimental FI investigations.

(2) An efficient, nanoscale detector would greatly enhance the prospects of molecular-beam-based microscopy, in which images are formed by scattered atoms or molecules rather than by the photons or electrons employed in conventional optical and electron microscopy.

Briefly pursuing the latter topic, it is clear that molecular beam microscopy (MBM), like any microscopy, requires an intense beam of the imaging particles, a means of focusing this beam, and a means of efficiently detecting the beam. Both scanning and imaging variants of MBM are possible. The spatial resolution of scanning MBM will be set by the size of a beam spot that is rastered across the target surface. A small spot requires a small source size and the ability to demagnify this to a sufficiently microscopic dimension. Micro- and even nanoscale molecular beam nozzles and skimmers can be fabricated by 'pulling' capillary tubing or hollow-core optical fibres [12, 13]. The beam flux decreases with cross-sectional nozzle area, however, making large numerical aperture optics and very efficient beam detection mandatory. Suitable mirrors can be formed from bent single crystals, and the design and development of such mirrors is progressing rapidly [14]. Thus the critical element in the development of scanning MBM is the detector, the primary demand being for high detection efficiency in order to compensate the limited intensity intrinsic to a scanning MBM source. It is hoped that field ionization clusters or arrays may offer this efficiency. In the second variant, imaging MBM, it is the detector that sets the spatial resolution. The beam source can be large, allowing the use of much smaller numerical aperture optics, such as Fresnel zone plate lenses [15]. Zone plates of 50 nm resolution ($f/\# \approx 500$) have been fabricated [16] and the current bottleneck is therefore again the detector. A 2D detector of high spatial resolution, as possible with an FI tip array, would be ideal. The question of bent crystal mirrors versus a zone plate lens is one of specific application rather than overall advantage. Bent crystals offer large numerical aperture and achromatic focusing but are applicable only with non-reactive beam species and must be used in a biaxial reflection geometry. Zone plate lenses can be used with any beam species and in a uniaxial transmission geometry, but are dispersive optical elements and have intrinsically small numerical apertures. With the demonstrated capabilities of zone plate focusing, MBM at optical resolution ($\leqslant 1\ \mu$m) is already feasible by use of a large 2D FI detector array of the sort fabricated by Spindt [10].

2. Field ionization detector (FID) measurements

We have recently carried out fairly extensive field ionization tip characterization at the Max-Planck-Institut für Strömungsforschung in Göttingen, Germany, using the field ionization detector of figure 1 [17]. The ionizer tip is situated inside a grounded copper housing that is cooled to liquid nitrogen temperature when in operation. The tip is held at a high positive potential, typically +4 kV with respect to the grounded housing for an FI needle of 20 nm tip radius. A supersonic beam impinges onto the tip at about 50° with respect to the shank axis. Gases can be bled into the FID vacuum chamber through a variable leak valve to raise the overall background pressure in the ionization region. Ions formed by field ionization of beam or background gases are drawn into a channeltron electron multiplier (CEM), the rim of which is typically at -2 kV with respect to the grounded housing. The output from the CEM, monitored using standard pulse counting techniques, is measured as a function of the beam nozzle pressure and/or test chamber pressure. Details of the measurements are presented elsewhere [17], and the results are summarized in table 1. The detector response is expressed in terms of an 'effective' cross-sectional detector area πb^2 based on the radius b required of an

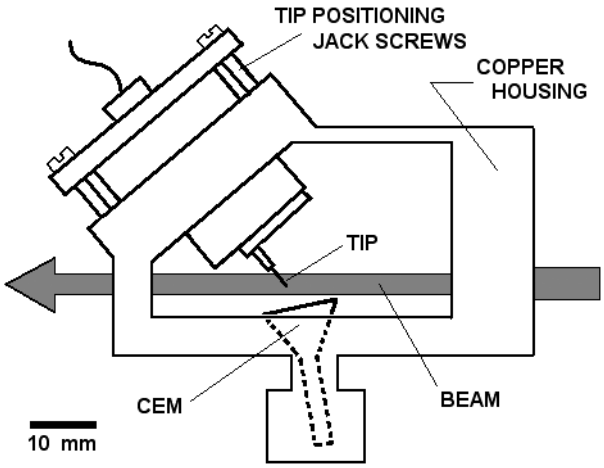

Figure 1. Plan view scale drawing of the field ionization detector used in measurements at the Max-Planck-Institut für Strömungsforschung [17].

Table 1. FID detection of supersonic and effusive beams.

Description of FID measurement	Measured sensitivity (cnts s^{-1} Pa^{-1})	Measured eff. area (nm^2)
Static residual gas, 295 K 19 nm tip at ∼6 kV and 80 K Doak *et al* [17]	6.55×10^9	53 000 est.
Static He gas, 295 K 19 nm tip at ∼6 kV and 80 K Doak *et al* [17]	1.09×10^9	3550
Supersonic He beam, 295 K 19 nm tip at ∼6 kV and 80 K Doak *et al* [17]	—	49
Effusive He beam, <4 K 10–70 nm tip at 5–18 kV and ∼4 K McWane and Oates [6]	—	200 000
Effusive He, Ar, and N_2 beams, 295 K 100 nm tip at 20 kV and 295 K Johnston and King [4]	$\sim 5 \times 10^{10}$	$\sim 10^6$

ideal, 100% efficient spherical ionization region in order to deliver the same number of ions per second as the measured signal count rate [6, 17]. This characterization disregards the true tip shape, and lumps together the separate effects of detector collection volume and ionization probability within this volume. It also ignores transport of atoms to the tip by any means other than direct impact from the beam/background gas, specifically via diffusion along the tip shank. Since the experiments do not separate out these individual effects, it is a meaningful comparative quantity. Our effective detector area was determined by a linear fit to the nozzle or background pressure dependences of the CEM signal [17]. An absolute calibration of the beam intensity, e.g. by a calibrated stagnation pressure measurement [18], was not possible with the

Göttingen apparatus. McWane and Oates [6] employed the same definition of effective area but calculated their values relative to a measured beam intensity. Johnston and King [4] offer no specifics as to their definition or computation of effective detector area.

Table 1 exhibits striking differences in measured effective detector area. The area for a supersonic room temperature helium beam is much less than for a room temperature static helium gas. That area, in turn, is much less than those reported in the effusive beam measurements of the 1960s and 1970s. Note that the effective detector area for the supersonic beam is actually smaller than the physical size of the FI tip, indicating that the ionization probability is much less than unity over the actual active detector volume. Gas species, gas flow type (supersonic beam versus effusive beam versus static gas), beam/gas temperature, tip temperature, and tip radius all play a role in determining the measured effective detector area. It is apparent that modelling is necessary to sort out the various contributing factors. Two issues are of particular interest as discussed above, namely (1) the conditions under which an incoming molecule reaches the tip, and (2) the probability that a molecule reaching the tip is ionized. The former defines a base cross-sectional size for the detector. Multiplication by the latter delivers the effective detector area.

3. Overly simplistic but useful modelling

We start with the question of base cross-sectional detector area. The trajectory of a gas molecule passing near the tip can be obtained from classical orbital mechanics. For a neutral non-polar molecule, the relevant potential energy is that due to polarization of the molecule in the electric field of the tip,

$$U(r,\theta,\phi) = -\tfrac{1}{2}\alpha E(r,\theta,\phi)^2, \tag{1}$$

where α is the static polarizability of the molecule. For a molecule of mass m with kinetic energy E_0 far from the tip, conservation of energy requires

$$E_0 = U(r,\theta,\phi) + \tfrac{1}{2}mv_{\mathrm{tan}}^2(r,\theta,\phi) + \tfrac{1}{2}mv_{\mathrm{r}}^2(r,\theta,\phi), \tag{2}$$

where v_{tan} and v_{r} are the tangential and radial velocity components. To proceed, a functional form for the electric field of the tip is needed. Analytical expressions have been obtained by modelling the tip as, for example, a paraboloid, hyperboloid, or spherical end cap on a truncated cone[3]. For the purpose of developing simple analytical scaling formulae, we adopt an even cruder approximation, namely a simple sphere of radius R as shown in figure 2. Modelling the tip as a spherical object reduces the calculation to a central force problem. Conservation of orbital angular momentum $L = mv_{\mathrm{tan}}r$ allows the tangential kinetic energy to be incorporated into an effective potential $U_{\mathrm{eff}}(r)$, delivering a simple 1D equation in r,

$$E_0 = U_{\mathrm{eff}}(r) + \tfrac{1}{2}mv_{\mathrm{r}}^2(r), \tag{3}$$

where

$$U_{\mathrm{eff}}(r) = -\frac{1}{2}\alpha E(r)^2 + \frac{L^2}{2mr^2}. \tag{4}$$

The electric field outside an isolated conducting sphere of radius R is

$$E(r) = \frac{V_0 R}{r^2}, \tag{5}$$

[3] See, for example, [7] (pp 41–19) and references therein.

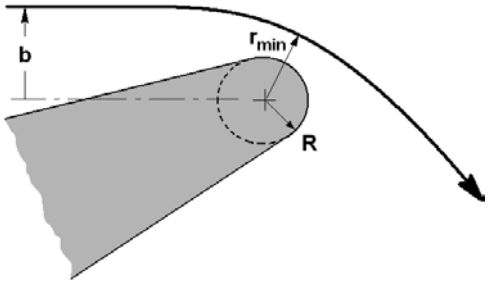

Figure 2. A gas molecule following the trajectory specified by the impact parameter b to pass through the radius of closest approach $r_{\min}$ near a field ionization tip, modelled as a sphere of radius R.

where V_0 is the potential applied to the sphere. Inserting this into equation (4) and expressing $L = mv_0 b$ in terms of $E_0 = 1/2mv_0^2$, the effective potential energy becomes

$$U_{\text{eff}}(r) = -\frac{1}{2}\alpha\left(\frac{V_0 R}{r^2}\right)^2 + \frac{E_0 b^2}{r^2}. \tag{6}$$

This potential displays a 'centrifugal barrier' at a position r^* given by

$$r^* = \sqrt{\frac{\alpha V_0^2}{E_0 b^2}}R. \tag{7}$$

$U_{\text{eff}}(r)$ is positive and repulsive at large r, rises to a positive maximum at r^*, and drops rapidly to negative values at still smaller r. Examples of $U_{\text{eff}}(r)$ are plotted in figure 3 for helium atoms incident onto a spherical tip at velocities corresponding to supersonic nozzle temperatures of 295, 77, and 4 K. Rewriting $U_{\text{eff}}(r)$ in terms of r^*,

$$U_{\text{eff}}(r) = \frac{E_0 b^2}{r^2}\left[1 - \frac{r^{*2}}{2r^2}\right]. \tag{8}$$

Inserting r^*, the barrier height is found to be

$$U_{\text{eff}}(r^*) \equiv U^*_{\text{eff}} = \frac{(E_0 b^2)^2}{2\alpha V_0^2 R^2}. \tag{9}$$

The barrier therefore increases rapidly with E_0 and b. The height of this barrier (relative to the incident energy) and its position (relative to the tip radius) will determine whether an impinging gas molecule can reach the tip (more exactly, whether it reaches the region of maximum tunnelling probability some 3–4 Å above the tip surface).

A gas molecule with incident energy larger than the barrier height will always strike the surface. From the above expressions, this occurs at impact parameters less than a critical value b^* given by

$$b^* \equiv \left(\frac{2\alpha V_0^2 R^2}{E_0}\right)^{1/4}. \tag{10}$$

This b^* sets the base cross-sectional area of the tip. A molecule incident at $b > b^*$ cannot reach the tunnelling region at R and therefore cannot be ionized. Hence[4]

$$A^* = \pi(b^*)^2 = \pi\left(\frac{2\alpha}{E_0}\right)^{1/2} V_0 R. \tag{11}$$

[4] Pauly, [1] (p 233), takes $A^* = \pi r^{*2}$ rather than πb^{*2}, which reduces the effective area by a factor of $1/\sqrt{2}$ relative to that of equation (11).

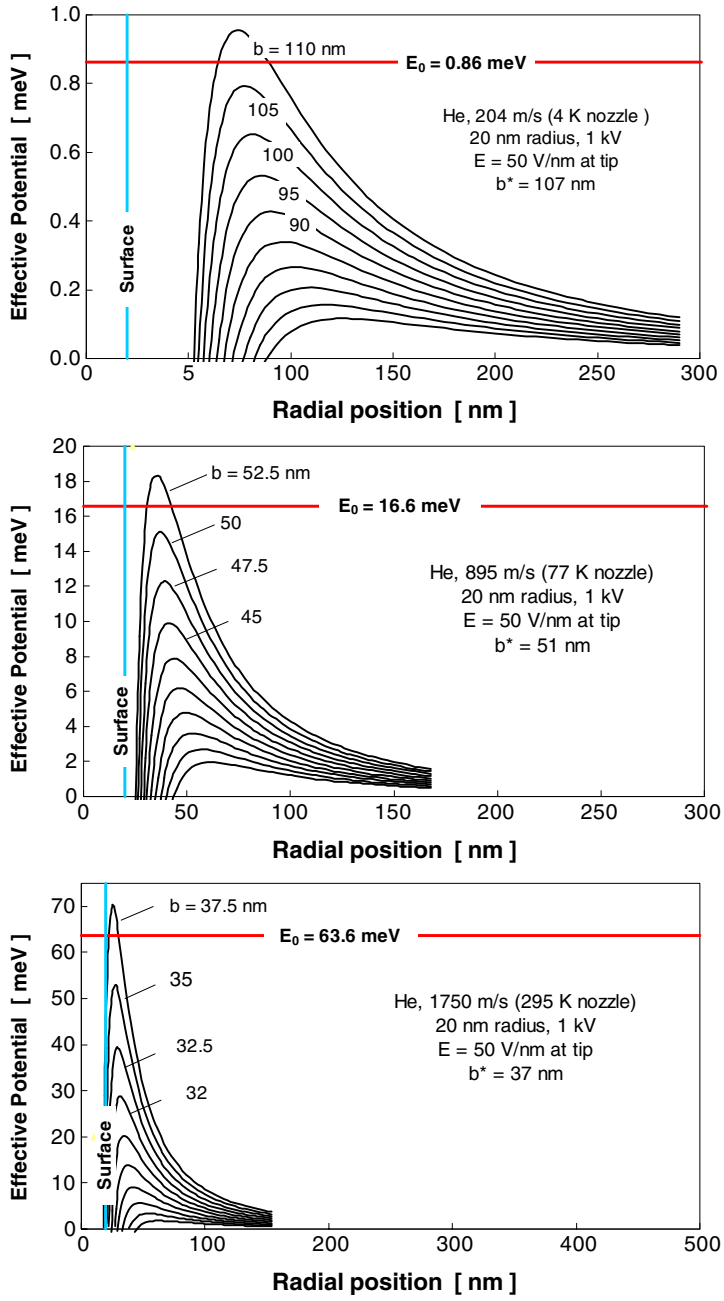

Figure 3. Centrifugal barriers for helium atoms incident at various velocities onto a 20 nm 'spherical' FI tip held at 1 kV with respect to its surroundings. The region of negative potential energy at small r is not shown. The barrier height increases with impact parameter b and, at sufficiently large b, rises above the incident energy E_0. At larger b, the atom cannot reach the tip region, so ionization is precluded. This critical value of impact parameter, denoted b^*, defines a base radius for the detection region.

(This figure is in colour only in the electronic version)

Table 2. Static polarizability α of common beam species (see footnote 5).

Species	$\alpha/4\pi\varepsilon_0$ (10^{-30} m^3)	α (C^2 m N^{-1})
He	0.205	2.28E−41
Ne	0.396	4.41E−41
Ar	1.640	1.82E−40
Kr	2.460	2.74E−40
Xe	3.990	4.44E−40
H	0.667	7.42E−41
Li	24.300	2.70E−39
Na	24.100	2.68E−39
K	43.400	4.83E−39
Cs	59.600	6.63E−39
H_2	0.787	8.76E−41
N_2	1.710	1.90E−40
O_2	1.562	1.74E−40
H_2O	1.501	1.67E−40

Within the scope of the simple 'spherical' tip model, the cross-sectional area of an FI detector is therefore largest for highly polarizable molecules of low kinetic energy and when using the largest possible tip radius and the highest possible voltage. For a given tip radius, field evaporation of the tip material ultimately sets an upper limits on the voltage [7]. The static polarizabilities of various common atomic beam gases are listed in table 2.[5] It is already obvious that helium, which is perhaps the species of greatest interest for much atomic beam research, will be the most difficult species to detect by field ionization.

If $b > b^*$, the centrifugal barrier becomes an obstacle, but the incoming atom can still strike the tip surface either by quantum mechanical tunnelling or if the tip surface lies outside the centrifugal barrier, $R > r^*$. In the latter cases it is also required that $E_0 > U_{\mathrm{eff}}(R)$. The first constraint places a lower limit on b and the second an upper limit:

$$\sqrt{\frac{\alpha V_0^2}{E_0}} < b < R\sqrt{1+\frac{\alpha V_0^2}{2E_0R^2}}. \tag{12}$$

These expressions define a capture radius when $b > b^*$. An appropriate expressions for the cross-sectional detector area can be worked out accordingly. Equations (10) and (11) rather than (12) are usually the relevant ones for low velocity atoms.

4. Modelling errors

The errors intrinsic to the spherical tip model can be assessed by noting a common technical formula for the E-field at the surface of a field ionization tip [7],

$$E(R) = \frac{V_0}{\kappa R}. \tag{13}$$

Here κ is the so-called 'field factor', a numerical factor that depends on the shank angle and that typically ranges from 5 to 8. Setting $\kappa = 1$ delivers $E(R)$ as in equation (5) above. Thus the spherical tip model overestimates the field strength at the tip surface by a factor of κ. In

[5] See, for example, the NIST Computational Chemistry Comparison and Benchmark DataBase, http://srdata.nist.gov/cccbdb/

addition, the true $E(r)$ will fall off with an inverse power of less than two for a real tip[6]. These observations prompt a corrected electric field of the form

$$E(r) = \frac{V_0}{\kappa}\frac{R^{2\beta-1}}{r^{2\beta}}, \tag{14}$$

which retains the correct dimensions and reduces to equation (5) for $\kappa = 1$ and $\beta = 1$. For this E-field, the barrier position is computed to be

$$r^* = \left(\frac{\beta\alpha V_0^2}{\kappa^2 E_0 b^2}\right)^{\frac{1}{2(2\beta-1)}} R, \tag{15}$$

and the barrier height

$$U^*_{\text{eff}} = \frac{E_0 b^2}{(r^*)^2}\left(1 - \frac{1}{2\beta(r^*)^{4(\beta-1)}}\right). \tag{16}$$

These dependences can be plotted numerically as a function of κ and β. If the barrier lies close to the tip, as in the middle and lower frames of figure 3, then $\beta \sim 1$ and the exponents are approximately those of the simple spherical tip modelling. The field factor dominates, reducing r^* by a factor of κ and A^* by a factor of κ^2. The functional dependences of equation (11) should then be reasonably accurate, but the effective detector area computed with that equation will be systematically high by a factor of 20–50. These systematic modelling errors can be seen in the plots of figure 3. Those calculations are for an applied voltage of only 1 kV, whereas our measurements were made at a voltage of 6 kV. Nonetheless, the E-field strength at the surface of the spherical tip (of 20 nm radius—comparable with the experiment) is already approaching the field evaporation limit (57 V nm^{-1} for tungsten at 0 K).

5. Interpretation of experimental measurements

The trends in measured effective detection area, table 1, agree reasonably well with the functional predictions of equation (11). The measured effective area should be smallest for the supersonic room temperature helium beam (lowest polarizability, highest incident energy). It should increase for a static helium gas (Maxwellian distribution providing low energy tails) and increase again for measurements on the test chamber background gas (consisting mostly of H_2O, with much higher polarizability than helium). The largest tip radius and highest applied potential should deliver the most signal. All of these trends are evident in the data.

The absolute numbers are even reasonable if the overestimate of the simple spherical tip model is taken into account. Equation (11) predicts $b^* = 90$ nm and $A^* = 25\,000$ nm^2 for helium from a room temperature supersonic nozzle impinging on a 20 nm radius tip held at 6 kV as in the experiment. Taking $\kappa = 6$ and removing factors of κ and κ^2, these reduce to 15 nm and 700 nm^2, respectively, compared with the measured values of 4 nm and 49 nm^2. This improves the agreement with experiment, but even so measured values appear to be smaller than expected. Indeed, as mentioned above, the measured cross-sectional detector area is actually smaller than the physical size of the tip, a clear indication that other considerations must enter. This introduces the second critical issue in the ionization process, namely the probability that a molecule reaching the tip is actually ionized.

We note in passing that the effective detector area predicted by equation (11) for a static helium gas at 4 K is 220 000 nm^2, which agrees very well with the data of Oates and McWane without being reduced by the factor of κ^2. Some reduction in correction factor can be understood: the top frame of figure 3 shows that the barrier in this instance is over

[6] See, for example, figure 2.4 of [7].

three tip radii removed from the centre of the tip, thus sampling an E-field gradient that is likely much shallower than the r^{-2} dependence of equation (5) and reducing the correction factor accordingly. This effect cannot reduce the correction factor to unity, however, so that the measured detector area is clearly larger than can be predicted within the simple model. Indeed, we will attribute this to shank diffusion, which is neglected in the simple spherical tip model.

Field ionization involves tunnelling through a barrier, and the probability of this, not surprisingly, can be much less than unity. Pauli exclusion precludes field ionization very close to the tip, where the energy level of the electron in the impinging molecule drops below the Fermi level of the tip and leaves no unoccupied states to tunnel into. The tunnelling probability decreases at large separation due to the increasing width of the tunnelling barrier. Accordingly, tunnelling is most likely in a narrow region typically situated 3–4 Å above the tip surface. For helium gas, the maximum tunnelling probability per pass through this region has been calculated to be 7%, 14%, and 29%, respectively, for tips at 80, 20, and 4 K [19]. If an impinging molecule is not ionized on its first impact with the surface, the decisive factor is whether it loses sufficient energy during that first collision to remain trapped in the polarization potential well. Once trapped, a molecule will eventually be ionized on some subsequent bounce. Thus, the overall ionization probability is greatly influenced by the trapping probability. Even if the helium atom scatters elastically, however, the slower speed and protracted time in the tunnelling region should greatly increase the ionization yield at lower incident velocities.

Trapping requires that the incoming molecule lose at least the difference between its incident energy and the barrier height, namely $E_0 - U^*_{\rm eff}$. This energy must be transferred to the tip (as opposed to internal degrees of freedom of the molecule) in order to ensure trapping. At thermal impact energies, lattice vibrations provide the only possible reservoir for this energy. Accordingly, the trapping probability increases with the phonon creation probability, which in turn increases with the mass and impact energy of the incident gas molecule. Since polarization forces accelerate the incoming molecule, the relevant impact energy is the incident energy $E_0 - U_{\rm eff}(R)$, which is greater than E_0 if $U_{\rm eff}(R)$ is negative. Maximum trapping is therefore expected for heavy, highly polarizable molecules having E_0 just greater than $U^*_{\rm eff}$, incident at small impact parameter b onto a tip of small radius so that $U_{\rm eff}(R)$ is strongly negative. Note that the polarizability of the molecule thereby plays a role not only in the centrifugal kinematics that determine the base detection area, equation (11), but also in the capture probability. As per equation (4), the maximum contribution of the polarization field to the impact energy occurs for $L = 0$ (i.e., for a head-on collision, $b = 0$). Using equation (13) with $\kappa = 6$ to compute the E-field at a real tip, the results are plotted for several species in figure 4. The dashed vertical line marks a tip radius of 20 nm. Reading off the intersection of the various curves with this line, it is seen that the upper limit on polarization-induced energy is 180, 340, and 580 meV for He, Ne, and H, respectively. Much larger gains are possible for more polarizable species: 1.4, 2.1, and 3.5 eV for Ar, Kr, and Xe, respectively. It is clear that the low polarizability of helium places it at the bottom of the list in trapping efficiency.

An addition of 180 eV for a helium atom is still supra-thermal. Note, however, that the impact energy is increased by this amount only for $b = 0$. At a finite impact parameter the contribution can be much less, particularly if the centrifugal barrier lies close to the tip. Extremes of the latter instance are evident in the plots of figure 3. In the top frame (4 K), the surface lies well within the barrier and even an atom impinging at b^* gains a substantial portion of the full polarization energy before striking the surface. One would therefore expect a high probability of inelastic scattering and trapping at 4 K. In the bottom frame (295 K), the surface actually intersects the effective potential at positive values for large impact parameter. In this

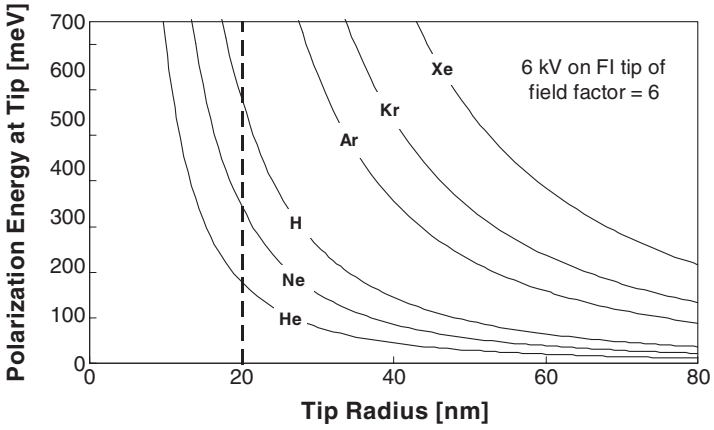

Figure 4. Maximum increase in impact energy due to acceleration in the polarization field, plotted as a function of tip radius for various gas species. An atom incident onto a true FI tip along the axis of the tip would gain this energy. The dashed vertical line marks a 20 nm radius.

case, an atom incident at b^* strikes the tip surface with less than its incident energy, significantly reducing the probability of inelastic scattering. It should be noted that the tunnelling probability depends critically on the velocity with which the atom passes through the region of optimum tunnelling, dropping off at higher velocity and approaching unity as the velocity approaches zero [19]. The increased tunnelling probability at lower velocity will, to some extent, offset the lower probability of trapping. This is of particular interest in the situation where the tip surface lies outside the centrifugal barrier. Should the classical turning point for a given incident energy lie at exactly the point of maximum tunnelling probability, impinging atoms would arrive in the tunnelling region with zero velocity and one would expect unity tunnelling probability.

Taking all of this into consideration, the measurements of table 1 make sense: the low mass and very quantum mechanical nature of helium lead to a high probability of elastic scattering upon impact with the tip surface. This elastic scattering can actually be enhanced in progressing from low beam velocity to high, due to $U_{\mathrm{eff}}(R)$ becoming less negative or even positive. Of the measurements listed in table 1, the supersonic beam (which is essentially monoenergetic at $\sim$1700 m s^{-1}) will therefore be most susceptible to a high elastic scattering and low capture probability. The higher trapping probability of the low velocity Maxwellian tails of a static room temperature helium gas apparently suffices to raise its overall ionization probability to above that of the supersonic beam.

For heavy and polarizable gases one would expect more inelastic scattering, leading to a greater probability of capture and eventual field ionization. Experimental data appear to bear this out. Comparative measurements of FID signal as a function of static gas pressure for helium, air, and xenon are plotted in figure 5. As detailed elsewhere, these data were recorded by bleeding the desired gas into the FID vacuum chamber [17]. These data sets were recorded one immediately after the other under identical conditions apart from gas species. The upper frame shows the FID signal output versus gas pressure of each gas as measured with an ionization gauge and corrected for the gauge sensitivity to the given gas [17]. The pressure dependence is very linear in all cases. Slopes resulting from linear least squares fits are listed in the plot, these then being the FID sensitivities to the various gases. These sensitivities are plotted in the lower frame as a function of the polarizability of the gases, table 2. Should the

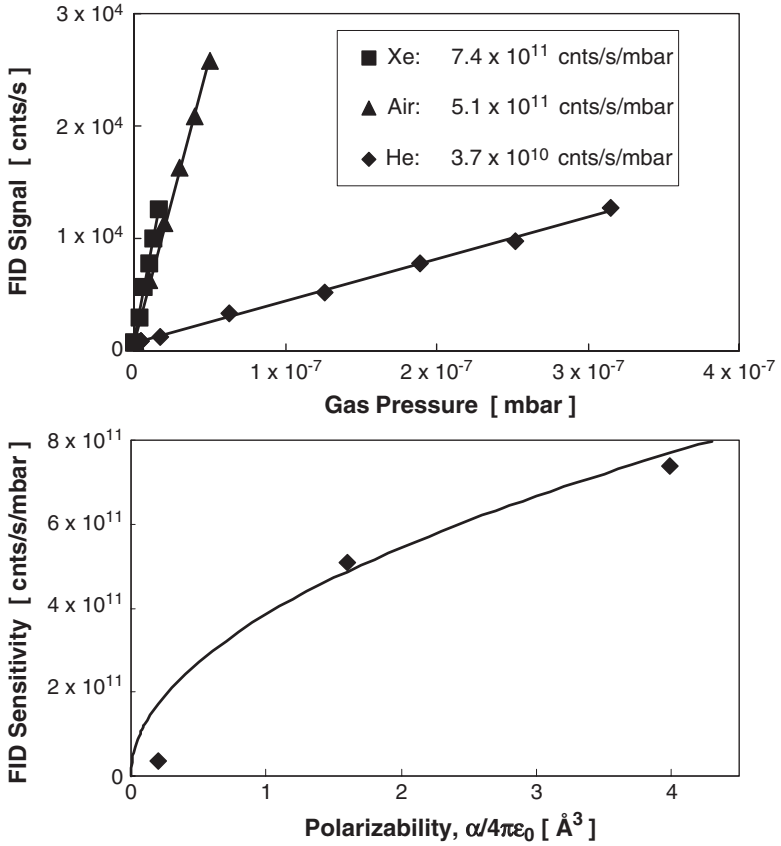

Figure 5. Experimental FID sensitivities for He, Xe, and air gases given by slopes of linear FID signal versus pressure curves, upper frame. These sensitivities are plotted as a function of species polarizability, bottom frame. A square root dependence can be passed through the upper two points, in agreement with equation (11) but this lies well above the measured sensitivity for helium (1 mbar = 100 Pa).

FID sensitivity be dominated by A^*, then equation (11) predicts a square root dependence on polarizability. A square root curve can be passed fairly accurately through the points for air and Xe, as seen in the lower frame, but this curve lies well above the point for helium, by almost a factor of five. We interpret this as a real effect due to the smaller capture probability of helium, due to its higher probability of scattering elastically from the tip and escaping ionization.

Increased tunnelling and ionization can increase the effective FID detection area, but only up to the base value A^* of equation (11). To explain the even larger effective areas measured at cryogenic temperature by McWane and Oates, it is therefore necessary to invoke effects neglected in the modelling up to this point. In particular, the arrival of molecules by means other than direct impact from gas surrounding the tip must be considered. We suspect that these large effective areas result from adsorption of impinging atoms onto the needle shank with subsequent diffusion along the shank to the tip, where they can then be field ionized. The polarization potential well along the shank is not nearly as strong as at the tip, but still much deeper than the attractive gas–surface interaction well. Thus adsorption onto and diffusion along the shank are enhanced by the presence of the applied potential. Supporting evidence

for this implication of shank diffusion comes from McWane and Oates themselves, who report that the temporal response of their tip was very slow (∼100 ms) with the tip at ∼2 K and that it was necessary to heat the tip to 'considerably warmer' temperatures in order to improve the time response to a value (<0.3 ms) that allowed TOF measurements to be made [6]. In contrast, our TOF measurements on a room temperature supersonic beam using an 80 K tip gave an upper limit on FID temporal response of about 1 μs [17]. Thus it seems fairly clear that significant shank diffusion was present in the cryogenic measurements, even with the heated tip. Since the effective cross-sectional area of the shank can easily exceed that of the polarization field, shank diffusion can significantly enhance the overall FID signal over that due to gas phase supply only.

If indeed an adsorbed layer of helium is present on the shank, it is worth noting that the inelastic scattering probability is greatly enhanced—possibly to near unity—if an impinging helium atom strikes an adsorbed, accommodated helium atom rather than a tungsten atom. Thus an adsorbed layer near the tip may significantly enhance the capture probability of atoms arriving from the gas phase, further improving the overall FID sensitivity. This, in fact, may also contribute to the higher effective detector areas measured by McWane and Oates.

6. The velocity dependence of field ionization dependence

A last puzzle in the overall picture is the apparent lack of a velocity dependence in the FID TOF curves as reported by McWane and Oates [6]. The simple modelling of equation (11) predicts a v_0^{-1} dependence of the effective FI detector area on the incident velocity v_0 of an impinging molecule. There is also a velocity dependence to the tunnelling probability, which drops off with increasing atom velocity in a more complicated fashion [19]. Finally, the capture probability may also decrease with increasing velocity due to the decrease in polarization-enhanced impact energy as the centrifugal barrier moves inward. Regardless of which factor dominates, one would expect a strong inverse velocity dependence to the detector response, and this should show up in the overall shape of the measured TOF traces. In contrast, McWane and Oates report no velocity dependence in TOF traces measured in at least 200 data sets with a dozen different tips and at effusive beam temperatures ranging from 0.3 to 4 K. There appear to be some irregularities in the McWane and Oates TOF analysis, however. The TOF distribution for an effusive Maxwellian beam with a detector velocity response of v_0^n is—as correctly given by McWane and Oates

$$A(t) = A_0 \frac{\tau^{4+n}}{t^{5+n}} \mathrm{e}^{-\tau^2/t^2},$$

where t is the flight time and $\tau = l/v$, with l the flight path and $v = (2kT/M)^{1/2}$ the most probable speed of a static gas Maxwellian speed distribution[7]. The position of the peak in the TOF distribution is found by setting $\mathrm{d}A(t)/\mathrm{d}t = 0$ to yield

$$t_{\mathrm{peak}} = \sqrt{\frac{2}{5+n}} \frac{l}{v}.$$

Thus, for $n = 0$ (no velocity dependence), $n = -1$, and -2, etc, it follows that $t_{\mathrm{peak}} = 0.63l/v$, $0.71l/v$, and $0.82l/v$, etc. The TOF peaks in figure 3 of the McWane and Oates paper [6] both clearly lie at $t_{\mathrm{peak}} = l/v$, which is the case only for $n = -3$. Thus it appears that their TOF delay was set by incorrectly placing the measured TOF peaks at $t_{\mathrm{peak}} = l/v$.

[7] Note that the most probable speed for an effusive Maxwellian is actually $v_{\mathrm{effusive}} = (3kT/M)^{1/2}$, or faster than v by a factor of $(3/2)^{1/2}$. This comes from the v^3 prefactor in the effusive velocity distribution as opposed to v^2 for the static gas.

This is not a trivial point, since the position and width of a Maxwellian distribution (for either a static or effusing gas) are correlated: if an incorrect t_{peak} yields a good fit to the peak width, then the width must *ipso facto* be wrong. Accordingly, McWane and Oates' seemingly good fit of their velocity-independent curve to the experimental data must be patently fortuitous. Upon shifting the TOF origin to the correct flight time (1.02 ms on McWane and Oates' plots), the experimental TOF curve is far too broad to be fitted with the velocity-independent ($n = 0$) TOF distribution. A $v^{-1.8}$ dependence gives about the correct TOF peak width, but must be shifted by 0.6 ms to shorter flight times in order to fit the peak position correctly. This implies that the assumed temperature is too low, that the distribution is non-Maxwellian, that there are additional errors in the TOF calibration, or some combination of these. If the source temperature is taken as a free parameter, a reasonable fit of both peak width and peak position can be obtained, for example, for a $v^{-2.5}$ velocity dependence and a 3 K source. We do not advocate these specific values, but quote them only to point out that the McWane and Oates data, when corrected for an improper TOF delay, seem to actually imply a velocity dependence to the overall ionization probability. It is risky, of course, to reassess 30-year-old data with no details as to the original fitting procedure. More valuable would be a remeasurement of the TOF spectra, using modern TOF capabilities.

An objective TOF calibration must be based on explicit measurements of zero flight time, chopper phase angle, ion draw-out delays, and electronic delays [20], rather than on assumed properties of the beam that is actually under investigation. Only then does a fit to the experimental TOF spectrum deliver unbiased information. In the present case, n, T, and even the basic form of the TOF distribution function are all nominally unknown, and must be taken as adjustable parameters in a TOF fit. Nonetheless, an objective fit would probably make it apparent whether the expected Maxwellian distribution is relevant and, if so, what values of n and T are appropriate. A properly calibrated TOF measurement would also allow shank diffusion to be critically assessed, since its presence would alter the TOF spectrum systematically as a function of shank temperature.

7. Summary and prognosis

It would appear that a cautious application of an overly simplified model can deliver useful insight into the possibilities and limitations of field ionization detection. These insights transfer to the more complicated geometry of an actual FI tip. The basic questions remain the same: Will the trajectory of a given molecule bring it within electron tunnelling reach of the tip? If so, what is the net tunnelling probability, integrated along the trajectory? If the trajectory brings the molecule into collision with the surface, what is the probability that it transfers sufficient energy and/or momentum to become trapped in the polarization well? Are there other pathways to the tunnelling region other than by direct impact from the gas phase?

For any molecule passing near a real field ionization tip, classical orbital mechanics will still determine whether the molecule reaches the tip or not. Polarization forces will bend the trajectory towards the tip, but will clearly bring the molecule within tunnelling range only for sufficiently low incident energy and/or for a sufficiently small skew separation between tip axis and initial line of travel. To improve upon the simple model, the impact cross-section of the tip must be obtained by an appropriate average over all possible kinematic parameters. The electric field of a real tip depends in a complicated fashion on r, θ, and ϕ, but reasonably good analytical expressions are available [7] and could be used to compute trajectories numerically as input for Monte Carlo averaging. This would be a manageable and useful exercise, given that the resulting cross-sectional area sets an upper limit on the overall ionization yield of the tip. The case of a supersonic beam (monodirectional and monoenergetic) would be especially easy to treat.

A proper calculation of the ionization probability of those molecules that reach the tip would be more challenging. Simple 1D calculations of tunnelling probability [19] would probably suffice, so the difficulty would lie in computations of the inelastic scattering and capture probability. The impact kinematics are far from simple, encompassing impact velocities from zero to supra-thermal and angles from near-normal to glancing angle. Simple models of phonon excitation might make the problem tractable.

The simple model of a spherical tip predicts, equation (11), that the base impact cross-section of the tip will increase with polarizability, tip potential, and tip radius and that it will decrease with incident energy. It also predicts, figure 4, that more polarizable species will gain more energy as they transit the polarization field, increasing their likelihood of scattering inelastically and becoming trapped. Existing models of tunnelling predict higher tunnelling probability at lower impact velocities [19]. Applying these predictions in a cautious, semi-quantitative fashion, the overall conclusion is that the measured FI detector sensitivities and effective areas of table 1 do make sense. This is unfortunate from the point of view of helium detection, since the measured effective detector area is very low for the room temperature supersonic helium beam. On the other hand, the simple modelling predicts significant increases in overall ionization as the energy of the beam is decreased, both because the base cross-sectional detector area increases and because the tunnelling and capture probabilities also increase. It may turn out that cryogenic temperature will be mandatory for helium beam microscopy. The question of adsorbate-enhanced sticking is certainly one that must be investigated. This mechanism would raise the overall ionization yield by increasing the capture probability, thus improving the output signal without sacrificing temporal response. In contrast, shank diffusion is probably to be avoided, as it would constrain temporal response.

Experimental measurements at cryogenic tip temperatures and with low velocity supersonic beams would be very instructive.

Acknowledgments

The author gratefully acknowledges support from the Deutsche Akademische Austauschdienst, the Fulbright Commission, and the Max-Planck-Gesellschaft at various times in the course of these studies.

References

[1] Pauly H 2000 *Atom Molecule, and Cluster Beams* vol 1 (Berlin: Springer) chapter 5
[2] DeKieviet M, Dubbers D, Klein M, Pieles U and Schmidt C 2000 Design and performance of a highly efficient mass spectrometer for molecular beams *Rev. Sci. Instrum.* **71** 2015–8
[3] Lafon R, Chaloupka J L, Sheehy B, Paul P M, Agostini P, Kulander K C and DiMauro L F 2001 Electron energy spectra from intense laser double ionization of helium *Phys. Rev. Lett.* **86** 2762–5
[4] Johnston W D Jr and King J G 1966 Field ionization detectors for molecular beams *Rev. Sci. Instrum.* **37** 475–6
[5] Woods R O and Fenn J B 1966 Field ionization gauge for molecular beam detection *Rev. Sci. Instrum.* **37** 917–8
[6] McWane J W and Oates D E 1974 Field ionizers as molecular beam detectors *Rev. Sci. Instrum.* **45** 1145–8
[7] Miller M K, Cerezo A, Hetherington M G and Smith G D W 1996 *Atom Probe Field Ion Microscopy* (Oxford: Clarendon) chapter 2 and references therein
[8] Becky H D 1977 *Principles of Field Ionization and Field Desorption Mass Spectrometry* (New York: Pergamon) Prokai L 1990 *Field Desorption Mass Spectrometry* (New York: Dekker)
[9] Riley D J, Mann M, MacLaren D A, Dastoor P C, Teo K B K, Amaratunga G A J and Milne W 2003 Helium detection via field ionization from carbon nanotubes *Nano Lett.* **3** 1455–8
[10] Spindt C A 1992 Microfabricated field-emission and field-ionization sources *Surf. Sci.* **266** 145–54
[11] Schwoebel P R, Spindt C A, Holland C E and Panitz J A 2001 Field emission cleaning and annealing of microfabricated coldcathodes *J. Vac. Sci. Technol.* B **19** 980–7

[12] Braun J, Day P K, Toennies J P, Witte G and Neher E 1997 Micrometer-sized nozzles and skimmers for the production of supersonic He atom beams *Rev. Sci. Instrum.* **68** 3001–9
[13] Cook A M, Turner J, Grams M and Doak R B 2004 Characterization of miniature supersonic beam nozzles pulled from fused silica capillary tubing, unpublished
[14] See MacLaren D A, Holst B, Riley D J and Allison W 2003 Focusing elements and design considerations for a scanning helium microscope *Surf. Rev. Lett.* **10** 249–55 and references therein
[15] See Doak R B, Grisenti R E, Rehbein S, Schmahl G, Toennies J P and Wöll Ch 1999 Towards realization of an atomic de Broglie microscope: helium atom focusing using Fresnel zone plates *Phys. Rev. Lett.* **83** 4229–32 and references therein
[16] Rehbein S 1999 unpublished
[17] Doak R B, Ekinci Y, Holst B and Toennies J P 2004 Field ionization detection of supersonic molecular beams *Rev. Sci. Instrum.* **75** 405–14
[18] Doak R B 1992 Single-phonon inelastic helium scattering *Atomic and Molecular Beams Methods* vol 2, ed G Scoles (Oxford: Oxford University Press) chapter 14
[19] Haydock R and Kingham D R 1981 *Surf. Sci.* **103** 239
[20] Doak R B and Nguyen D B 1988 Absolute calibration of an atomic helium beam time-of-flight apparatus by flight path variation *Rev. Sci. Instrum.* **59** 1957–64